ELSEVIER

In Collaboration with
the Netherlands Institute for Sea Research

JOURNAL OF SEA RESEARCH

Journal of Sea Research 46 (2001) 117–132

www.elsevier.com/locate/seares

Dynamical impacts associated with radiation boundary conditions

Elbio D. Palma[a,*], Ricardo P. Matano[b]

[a]*Departamento de Física, Universidad Nacional del Sur, Av. Alem 1253, 8000 Bahía Blanca, Argentina*
[b]*College of Oceanic & Atmospheric Sciences, Oregon State University, 104 Ocean Admin Building, Corvallis, OR 97331-5503, USA*

Received 29 March 2000; accepted 8 March 2001

Abstract

It is well known that the use of radiation conditions for the non-linear shallow water equations can lead to an incorrect model response in a variety of dynamical settings. In this study, we show that conditions aimed to handle the radiation of outgoing disturbances are not sufficient to ensure the correct mass and energy fluxes at the open boundaries in long-term wind-forced flows and short-term simulations dominated by wave radiation. Moreover, the mass and energy flux imbalance across the open boundaries introduces an accumulating error that deteriorates the interior solution. To ameliorate this problem, we tested damped schemes and integral constraints on surface elevation and mass flux. A comparison of the model results indicates that the proposed schemes improved the overall performance of the open boundary conditions in a series of experiments conducted in a rotating channel, although there are limitations when the oceanic response consists of dispersive wave packets. The practical experience gained from the idealised studies shows that a modified gravity wave is the only scheme that provides a reasonable response in all cases studied. It is also found that consistent with the ill-posedness of the analytical problem, the numerical behaviour of the corrected schemes depends on the nature of the problem to be investigated.

Keywords: Coastal oceanography; Mathematical modelling; Boundary conditions; Open boundary conditions; Radiation conditions; Shelf dynamics

1. Introduction

Radiation conditions have been used in computational fluid dynamics well beyond its theoretical range of limitation (i.e. for flows obeying hyperbolic equations). Among the reasons for its widespread use are its easy implementation and reported success. Originally suggested by Sommerfeld (1949), radiation conditions can be generically written as:

$$\frac{\partial \phi}{\partial t} + C_\phi \frac{\partial \phi}{\partial n} = 0 \qquad (1)$$

where C_ϕ is the local phase speed of the dependent variable ϕ; t, the time and n is the coordinate perpendicular to the open boundary.

It has been observed in several numerical studies that under certain circumstances, the prescribed radiation open boundary conditions (OBCs) lead to spurious changes of mass in the interior domain. Blumberg and Khanta (1985) proposed a modified version of Eq. (1) based on a numerical scheme originally developed by Orlanski (1976). The new scheme was then used to set up a prognostic simulation of the South Atlantic Bight with tidal and wind forcing using a regional version of the Princeton Ocean Model (POM). They reported a steady emptying of the basin for a pure radiation condition with no

* Corresponding author.
E-mail address: uspalma@criba.edu.ar (E.D. Palma).

1385-1101/01/$ - see front matter
PII: S1385-1101(01)00076-4

boundary forcing. Chang (1994) studied the propagation of Kelvin and Rossby waves in a meridional channel with a linearised two-layer shallow water model applying Orlanski's scheme. The simulations with the pure outflow radiation condition produced a steady filling of the basin. Johnsen and Lynch (1995) described a series of numerical experiments conducted to study the behaviour of several radiation conditions as applied to a barotropic finite element model. The results using a first order discretisation of Eq. (1) showed a spurious filling of the basin under constant along-shore wind stress forcing. Palma and Matano (1998) implemented and tested different types of OBCs for the barotropic mode of POM employing a zonal channel. They found artificial changes in the basin average mean sea level when using radiation conditions in cases where the oceanic response consists in dispersive wave packets.

In this study, we will test a suite of radiation conditions applied to the shallow water equations to identify and offer solutions to some of the reported problems. The focus will be on passive OBCs where the response of the flow at the open boundaries is determined by the interior circulation. The numerical experiments are designed to emphasise flow conditions dominated by wind forcing and/or wave radiation.

This article has been organised as follows: Section 2 contains a description of the numerical model and the OBCs schemes. Section 3 describes the numerical experiments and, finally, Section 4 summarises and discusses the results.

2. Numerical model

The numerical model to be used in our experiments is the Princeton Ocean Model (POM). It solves the three-dimensional primitive equations in finite differences on an Arakawa C grid. The numerical scheme conserves linear and quadratic quantities, like mass and energy. It uses sigma coordinates in the vertical and curvilinear coordinates in the horizontal. Spatial differences are explicit in the horizontal and implicit in the vertical. A detailed description of the model can be found in Blumberg and Mellor (1987). In the following calculations, only the equations corresponding to the barotropic mode will be used:

$$\frac{\partial \eta}{\partial t} + \frac{\partial UD}{\partial x} + \frac{\partial VD}{\partial y} = 0$$

$$\frac{\partial UD}{\partial t} + \frac{\partial U^2 D}{\partial x} + \frac{\partial UVD}{\partial y} = -fVD + gD\frac{\partial \eta}{\partial x} = \tau_x^{\mathrm{b}} + \tau_x^{\mathrm{w}} + \frac{\partial}{\partial x}\left[H2A_{\mathrm{M}}\frac{\partial U}{\partial x}\right] + \frac{\partial}{\partial y}\left[HA_{\mathrm{M}}\left(\frac{\partial U}{\partial y} + \frac{\partial V}{\partial x}\right)\right]$$

$$\frac{\partial VD}{\partial t} + \frac{\partial UVD}{\partial x} + \frac{\partial V^2 D}{\partial y} = -fUD + gD\frac{\partial \eta}{\partial y} = \tau_y^{\mathrm{b}} + \tau_y^{\mathrm{w}} + \frac{\partial}{\partial y}\left[H2A_{\mathrm{M}}\frac{\partial V}{\partial y}\right] + \frac{\partial}{\partial x}\left[HA_{\mathrm{M}}\left(\frac{\partial U}{\partial y} + \frac{\partial V}{\partial x}\right)\right] \quad (2)$$

where η is the sea surface elevation, $\{U,V\}$, the horizontal components of the depth averaged velocity, H, the depth below mean sea level, D, the total depth, $f = 1.028 \times 10^{-4}$, the Coriolis parameter, g, gravity, $\{\tau_x^{\mathrm{b}}, \tau_y^{\mathrm{b}}\}$, the bottom stress components (the coefficient of bottom friction was 0.0025), $\{\tau_x^{\mathrm{w}}, \tau_y^{\mathrm{w}}\}$, the wind stress components and $A_{\mathrm{M}} = 200\ \mathrm{m^2\ s^{-1}}$, a constant horizontal mixing coefficient.

The numerical experiments were conducted in a zonal channel 1000 km long and 500 km wide, with a horizontal grid resolution of 20 km. The channel has two open boundaries on the western and eastern sides. Fig. 1 shows the two bottom configurations used in the experiments. These particular profiles were chosen to allow comparison between our results and previous experiments (Chapman, 1985; Tang and Grimshaw, 1996) and to resolve physical phenomena of particular interest in coastal oceanography (e.g. the propagation of continental shelf waves).

The OBCs tested in this study are variants of the Sommerfeld condition (1). The schemes considered can be divided into two groups:

(1) Fixed $C_\phi (= C_{\mathrm{o}})$. This approximation assumes that the waves approaching the open boundary are non-dispersive surface gravity waves (Chapman,

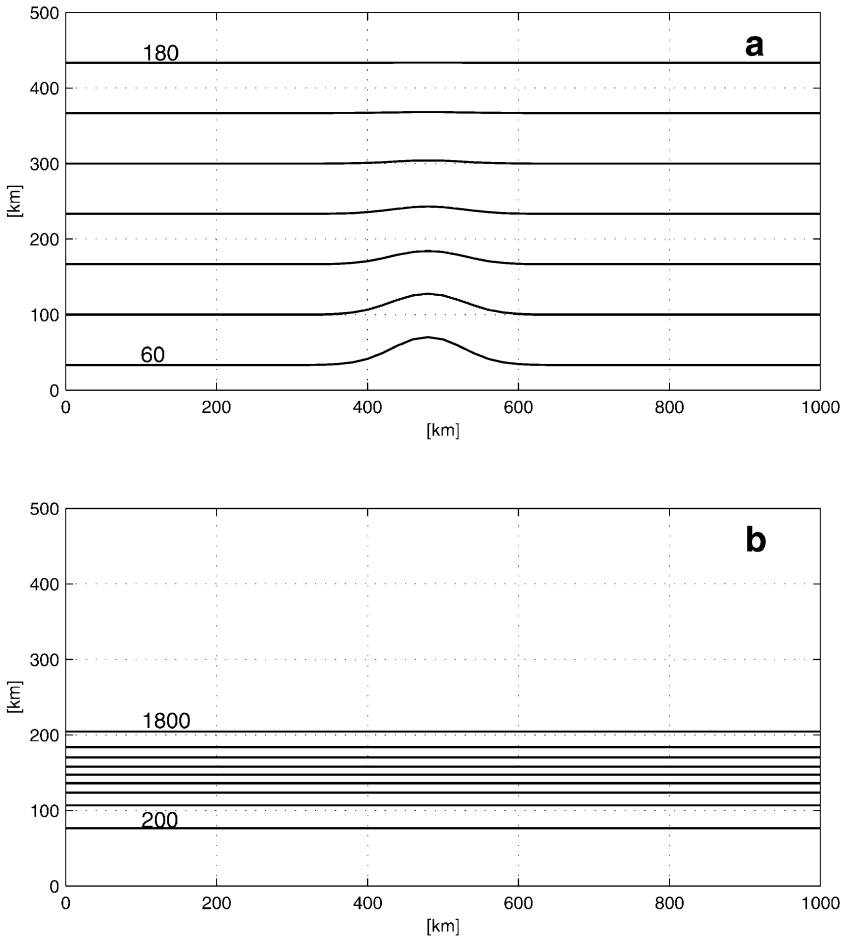

Fig. 1. Model bathymetry used in the numerical experiments. (a) Plan view of linear profile (along-shelf wind experiment). (b) Plan view of hyperbolic tangent profile (eddy relaxation and travelling storm experiments).

1985; Vastano and Reid, 1967). We tested the following variants:

GWI: A straightforward implementation of Eq. (1) with an implicit method and upstream scheme for the evaluation of the partial derivatives (Chapman, 1985).

BKI: It has been shown that in certain circumstances the implementation of GWI at the open boundaries can produce spurious changes in mean sea level (Blumberg and Khanta, 1985). To minimise this problem, Blumberg and Khanta developed a 'damped' version of the GWI scheme:

$$\frac{\partial \phi}{\partial t} + C_o \frac{\partial \phi}{\partial n} = -\frac{\phi - \phi_{ref}}{T_f} \tag{3}$$

where T_f is the relaxation time scale within which the numerical solution is restored to its reference value (ϕ_{ref}) at the open boundary. It will be shown that the selected value of T_f has a strong influence on the nature of the solution inside the domain.

FLA: This OBC was originally proposed by Flather (1976) and combines Eq. (1) with a one-dimensional version of the continuity equation to yield an equation for the normal velocity that allows conservation of mass in the interior domain. It can be written as:

$$U = U_o(t) \pm \frac{C_o}{H}[\eta - \eta_o(t)] \tag{4}$$

where U_o and η_o are prescribed values. The plus sign is applied at the eastern boundary while the minus

sign is used at the western open boundary. This OBC scheme is specified to account for the effects of outer regions (not modelled) to the degree possible through U_o and η_o, and differences from this are treated as a radiation condition to minimise reflections at the boundary of waves generated within the model domain. Since in the case of passive OBCs, the exact values of U_o and η_o are generally unknown, they are assumed to be zero at the boundary.

(2) Variable C_ϕ. Orlanski (1976) proposed to compute the phase speed of waves approaching the open boundary using a diagnostic version of Eq. (1), i.e.

$$C_\phi = -\frac{\partial\phi/\partial t}{\partial\phi/\partial n} \tag{5}$$

where the partial derivatives are evaluated at previous time steps and from interior values. The computed phase speed is then used in Eq. (1) for outflows and set to zero for inflows. Given its widespread use, we tested three different versions of Orlanski's condition. They are:

SOE: Miller and Thorpe (1981) modified the original Orlanski scheme using a forward scheme for time differences and an upstream scheme for space differences, which are more accurate.

ORI: Uses an implicit version of the original leap-frog time-splitting technique. This scheme showed the best performance of those tested by Chapman (1985), with a linear shallow-water model.

SRE: Tang and Grimshaw (1996) suggested this modification to the Orlanski scheme. They proposed a second order Lagrangian interpolation scheme to improve the accuracy and consistency of the original discretisation.

The numerical implementation of the OBCs schemes has two additional requirements: (a) the selection of the variables to be updated; (b) the selection of the boundary node to perform the discretisation. We found through numerical experimentation that the correct selection strongly depends on the chosen grid type (C grid) and model internal discretisation. For the scheme based on normal velocities (FLA), the OBCs were successfully applied at $I = 2$ and $I = I_M$, where I_M is the maximum number of nodes in the zonal direction. The scheme is complemented with a GWI scheme on surface elevation (η) and the tangential velocity component (V). For the remaining radiation schemes, we tested the following possibilities:

(i) Radiation for the three variables: the model response becomes unstable for non-linear flows.
(ii) Radiation on η and V and gradient condition (zero normal derivatives) on U at $I = 1$ and $I = I_M$: the variables are not properly updated and the interior solution resembles the response of a closed domain.
(iii) Radiation on η and V at $I = 2$ and $I = I_M - 1$ supplemented with a gradient condition for the normal velocity U gives the best results and therefore, is used in all the following numerical experiments. Similar conclusions are obtained using radiation on η and V at $I = 1$ and $I = I_M$ and computing U with a linearised version of the momentum equation.

3. Numerical experiments

To evaluate the performance of the different schemes, we conducted three numerical experiments: (1) a wind set-up, (2) relaxation to an initial perturbation, (3) the oceanic response to the passage of a travelling storm. The first experiment allows us to evaluate the performance of the different OBCs in strong advective flows with a non-steady state solution. The second experiment

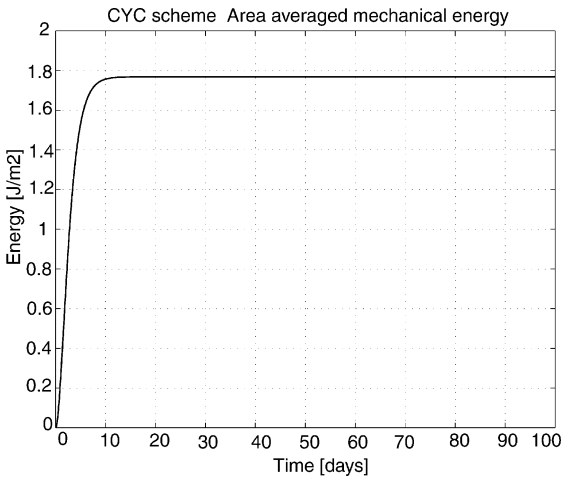

Fig. 2. Time evolution of basin averaged mechanical energy for the wind driven spin-up experiment using cyclic conditions.

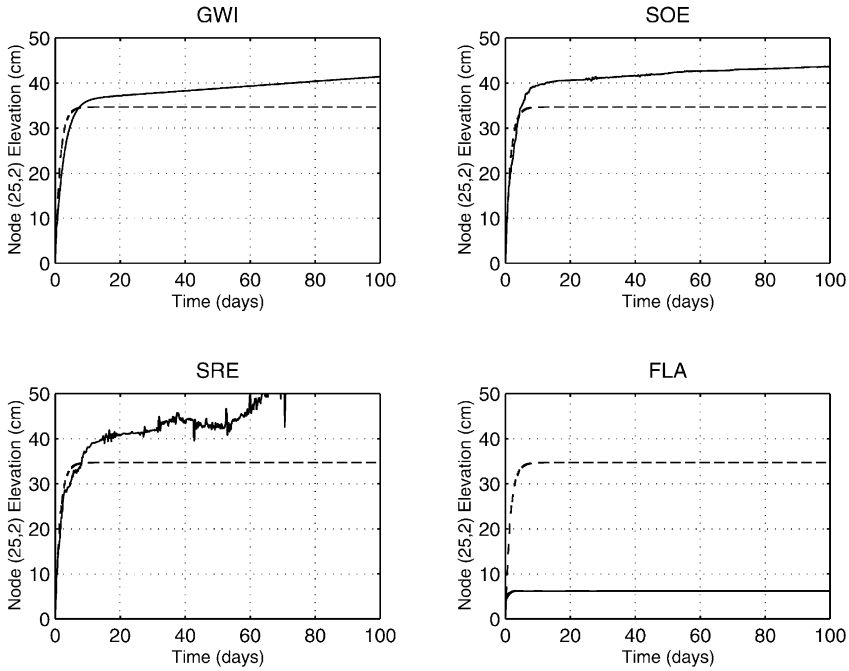

Fig. 3. Time series of sea surface elevation at a central coastal node from the wind-driven spin-up experiment. The dashed line is the result from the benchmark (cyclic OBC), solid lines are results obtained using the OBC scheme indicated on top of each panel. The results using ORI are similar to those shown in the SOE panel.

focuses on the behaviour of OBCs in flows dominated by wave radiation. Finally, the third experiment combines the characteristics of the previous two experiments, i.e. direct wind forcing and wave radiation.

3.1. Wind set-up

This experiment investigates the oceanic adjustment to the switch-on of a constant wind stress forcing. The uniform wind $t_x^w = 0.1$ Pa, is switched on at $t = 0$ and kept constant during the entire simulation. Fig. 1a shows the bottom topography used in this experiment. Since there is no analytical solution to this problem, we evaluated the performance of the different schemes using the results of a twin experiment in which the OBCs were replaced by cyclic conditions. Fig. 2 shows the time evolution of the averaged mechanical energy in the benchmark case. During the spin-up of the model, Ekman transports along the solid boundaries generate cross-shore pressure gradients that lead to an along-shore geostrophic flow. By day 10, the model reaches a steady state, where the energy input by the wind is dissipated by bottom friction.

The results of the different experiments are summarised in Fig. 3, which shows the time series of the coastal sea surface elevation in the middle of the channel. GWI, SOE, and ORI (not shown) show a slightly slower temporal evolution during the first week compared to the CYC condition, and a steady increase in sea surface elevation thereafter. This behaviour has also been reported by Chang (1994) in a long-term simulation with a two-layer shallow water finite difference model and by Johnsen and Lynch (1995) with a barotropic finite element model. Of all the schemes, SRE has the poorest performance. The solution is contaminated by the inward propagation of short waves, a constant increase of the sea surface elevation and the growth of instabilities. The solution using FLA reaches an incorrect steady state value after a short period; its numerical scheme prevents the normal evolution of the cross-shore surface slope at the open boundaries,

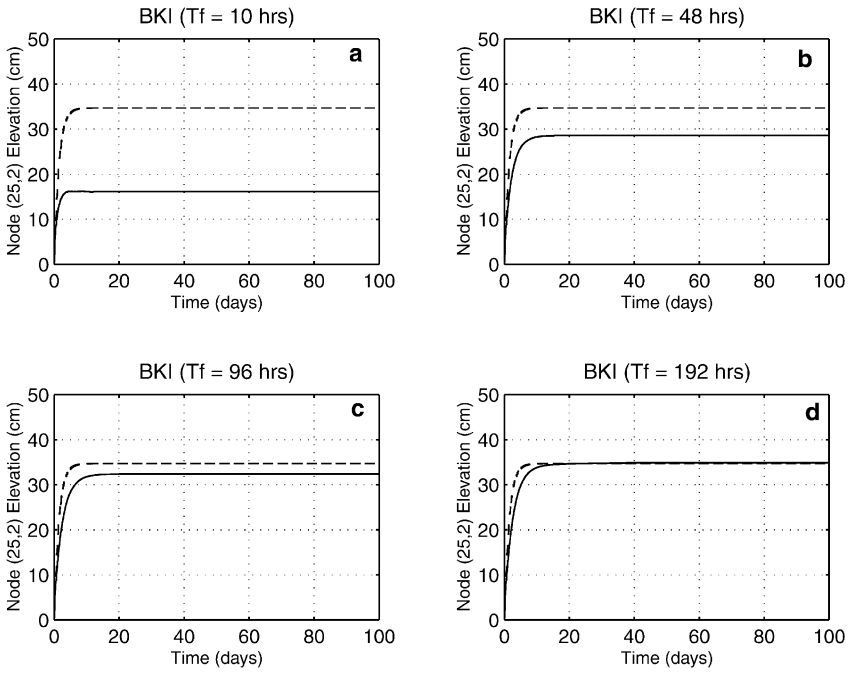

Fig. 4. As for Fig. 3 but showing results using the BKI scheme for different values of the time relaxation parameter (T_f).

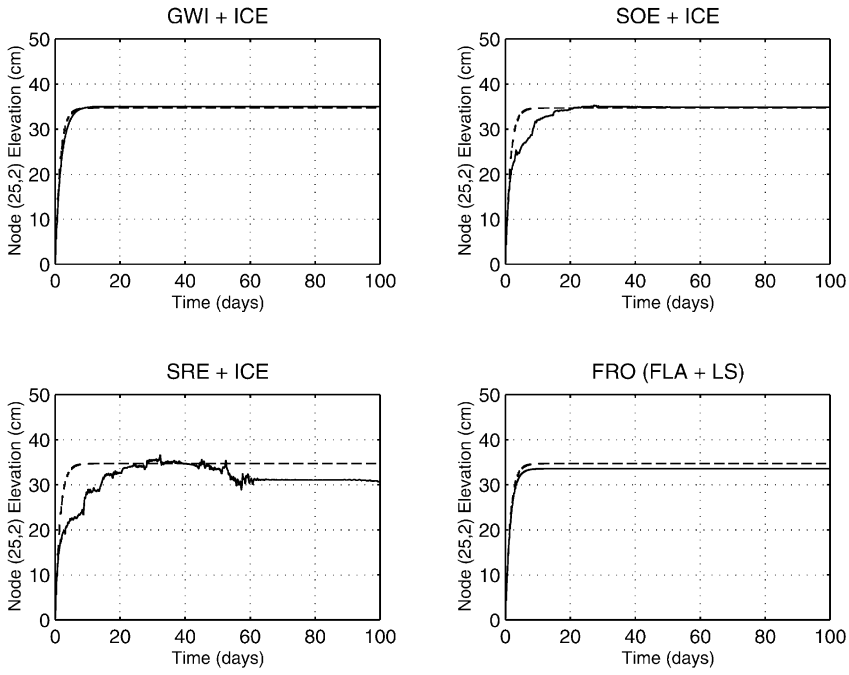

Fig. 5. As for Fig. 3 but showing results using the integral constraint on surface elevation (ICE) for SOE and SRE radiation conditions (ORI results are similar to SOE) and the FLA scheme with the local solution (LS).

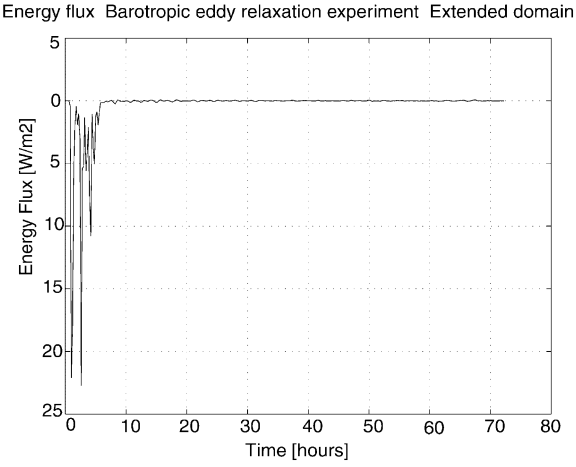

Fig. 6. The time evolution of the energy flux through the western boundary for the barotropic adjustment experiment (benchmark run).

which in turn reduces the along-shore transport (Hayashi et al., 1986).

As a first attempt to alleviate the steady filling of the basin, we employed the BKI scheme. Additional information is necessary to determine the appropriate value of T_f. According to Blumberg and Khanta (1985), T_f is related to the time it takes for a perturbation to cross the entire shelf. A numerical experiment where a symmetrical mound of water was released at the middle of the domain was employed to access this time scale. The experiment was conducted with the same bathymetry but on a zonal extended domain (10 000 km) to avoid the imposition of OBCs during simulation time (a detailed description of this experiment can be found in Palma and Matano (1998)). The time evolution of the energy flux through the eastern boundary shows that the perturbation takes approximately 5 h to reach the open boundary, suggesting a relaxation time scale T_f of 10 h. The energy flux is defined as:

$$\mathrm{EF} = (1/W)\int_0^W DU\left(g\eta + \frac{1}{2}U^2 + \frac{1}{2}V^2\right)\mathrm{d}y \qquad (6)$$

where W is the basin width. The results of the BKI scheme applied to the wind-forced experiment are shown in Fig. 4. BKI with $T_f = 10$ h stops the basin filling, but induces an excessive clamping of the boundary which in turn results in an improper decrease in elevation (Fig. 4a). Further increase of T_f improved the overall response (Fig. 4b and c) as expected. A time scale of four days seems to be an adequate compromise among the clamping and radiation characteristics of the scheme for this advection-dominated dynamical setting (Fig. 4d).

An alternative method to improve the performance of the different schemes is through the use of an integral constraint on sea surface elevation (ICE) which forces mass conservation at the boundaries i.e.

$$\int_0^W \eta\,\mathrm{d}y = 0 \qquad \text{at } x = 0, L \qquad (7)$$

All the experiments using ICE (GWI, SOE and ORI (not shown)) correctly reproduce the benchmark experiment (Fig. 5). Although ICE prevents the mass imbalance associated to SRE, the simulation does not reach the benchmark steady state after 100 days of simulation.

Although the FLA condition assumes that no information on the boundary was available and consequently U_o and η_o were set to zero in Eq. (4), an improvement to the performance of this scheme can be obtained by employing a local solution (LS) where the governing equations are linearised and all gradients in the alongshelf direction are neglected (Roed and Smedstad, 1984). With this correction, the FLA scheme also performs correctly, as seen in Fig. 5.

3.2. Barotropic adjustment

The objective of this experiment is to test the reflection properties of the different OBCs schemes in flows dominated by wave radiation. Following Tang and Grimshaw (1996), the experiment consists of the free (no forcing) adjustment of a kinetic energy input in a fluid otherwise at rest. The initial perturbation corresponds to a localised eddy of the form:

$$U_o(x,y) = \frac{1}{H}\frac{\partial\psi_o}{\partial y}, \qquad V_o(x,y) = -\frac{1}{H}\frac{\partial\psi_o}{\partial x},$$
$$\text{with } \psi_o = \psi_m \exp\left(-\frac{x^2}{R^2} - \frac{(y+y_o)^2}{R^2}\right) \qquad (8)$$

The eddy has maximum radial velocity $V_m = 0.86\psi_m/H_oR_o = 25$ cm/s, radius $R_o = 75$ km, and centred at $x = 500$ km, $y_o = 150$ km, where $H_o = H(y_o)$. The model topography is shown in Fig. 1b.

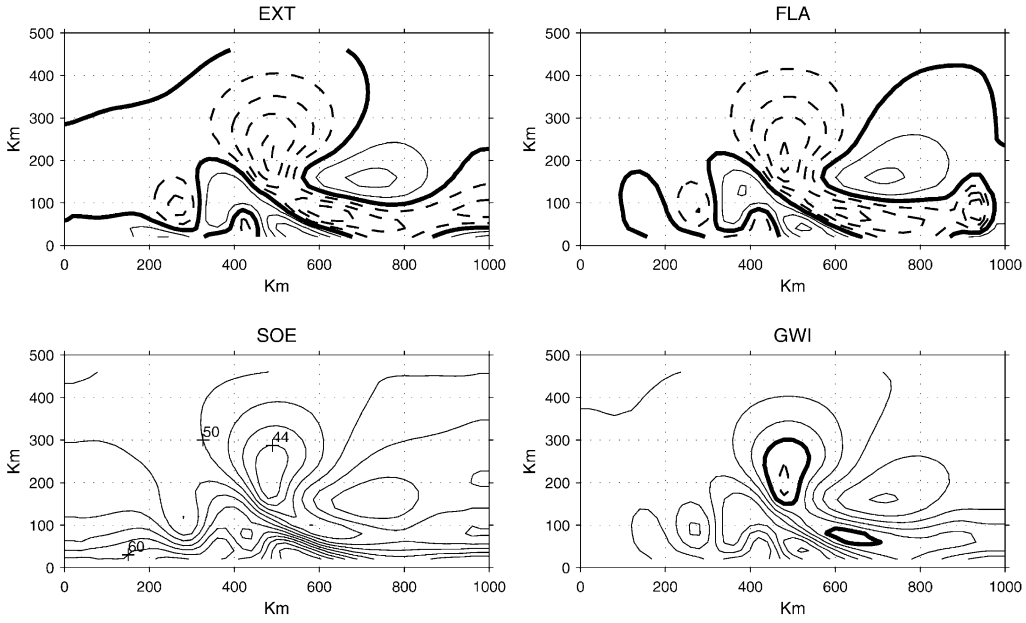

Fig. 7. Snapshots of sea surface elevation contours after 3 days from the barotropic relaxation experiment. The upper left panel shows the result from the extended domain experiment (EXT), other panels are results obtained using the OBC scheme indicated on top of each panel. Results using ORI and SRE are similar to those of SOE. Contour interval is 2 cm, dashed lines indicate negative values and the thick solid line is the zero elevation contour. Note that the averaged mean sea level is higher than zero for the SOE scheme.

The benchmark experiment for this test was conducted in a closed basin with a zonal extension of 10 000 km. The analysis was focused on the central 1000 km of the basin, and the time integration was stopped before reflections from the closed boundaries could reach the domain of interest. The results of the benchmark experiment are summarised in Fig. 6, which shows the time evolution of the energy flux across the western boundary. The oceanic adjustment to the initial perturbation is accomplished by the propagation of Kelvin waves which reaches $x = 0, L$ in about 1 h, followed by edge waves travelling in

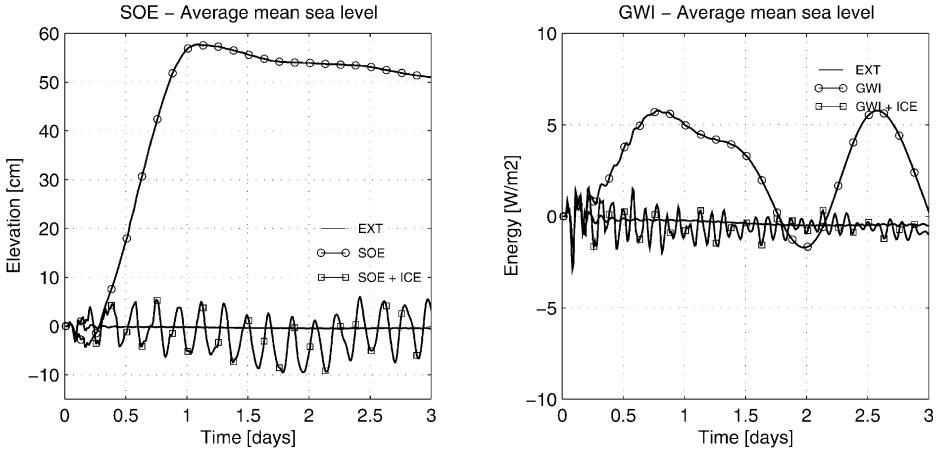

Fig. 8. Time series of area averaged mean sea level (AMSL) from the barotropic adjustment experiment.

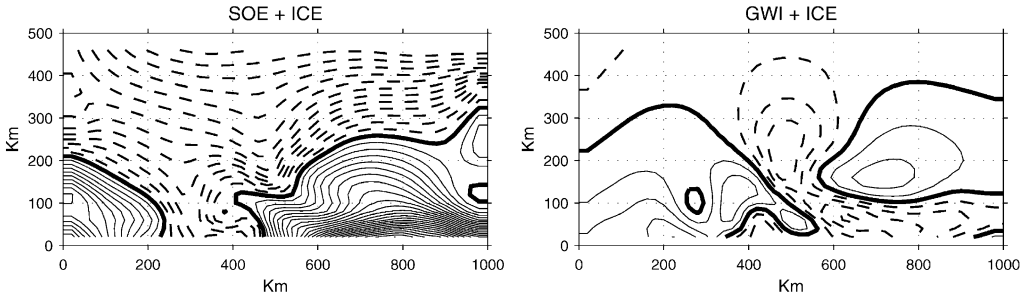

Fig. 9. As for Fig. 7 but showing results for SOE and GWI plus the integral constraint in elevation (ICE). Results using SRE and ORI are similar to those of SOE.

both directions. The continental shelf acts as a waveguide, and after about 10 h, most of the initial energy is lost by radiation.

The behaviour of the most representative OBCs is shown in Fig. 7, which shows the sea surface elevation field at day three of the simulation. For this particular experiment, the only OBC that simulates the response of the benchmark case is FLA, which allows the propagation of the incoming waves, although there is a small cross channel perturbation on the eastern open boundary. GWI, SOE, ORI and SRE (last two not shown) shows spurious sea surface displacement inside the computational domain.

The artificial filling of the basin during the numerical simulation can be quantified by the average mean sea level elevation:

$$\mathrm{AMSL} = \frac{1}{A_\mathrm{T}} \int_A \eta \, \mathrm{d}A \tag{9}$$

where A_T represents the area domain. This quantity is a measure of the mean sea level deviation away from the equilibrium depth (zero for the present

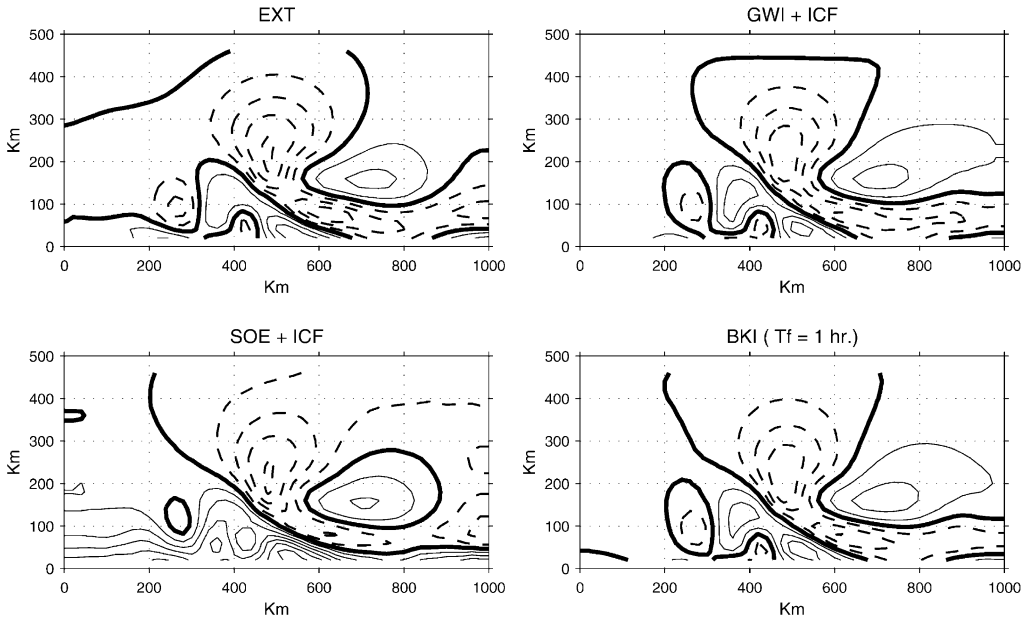

Fig. 10. As for Fig. 7 but showing results for SOE and GWI using the flux integral constraint (ICF). Results using ORI and SRE are similar to those of SOE. Also shown is the result for the BKI scheme with a time relaxation $T_f = 1$ h.

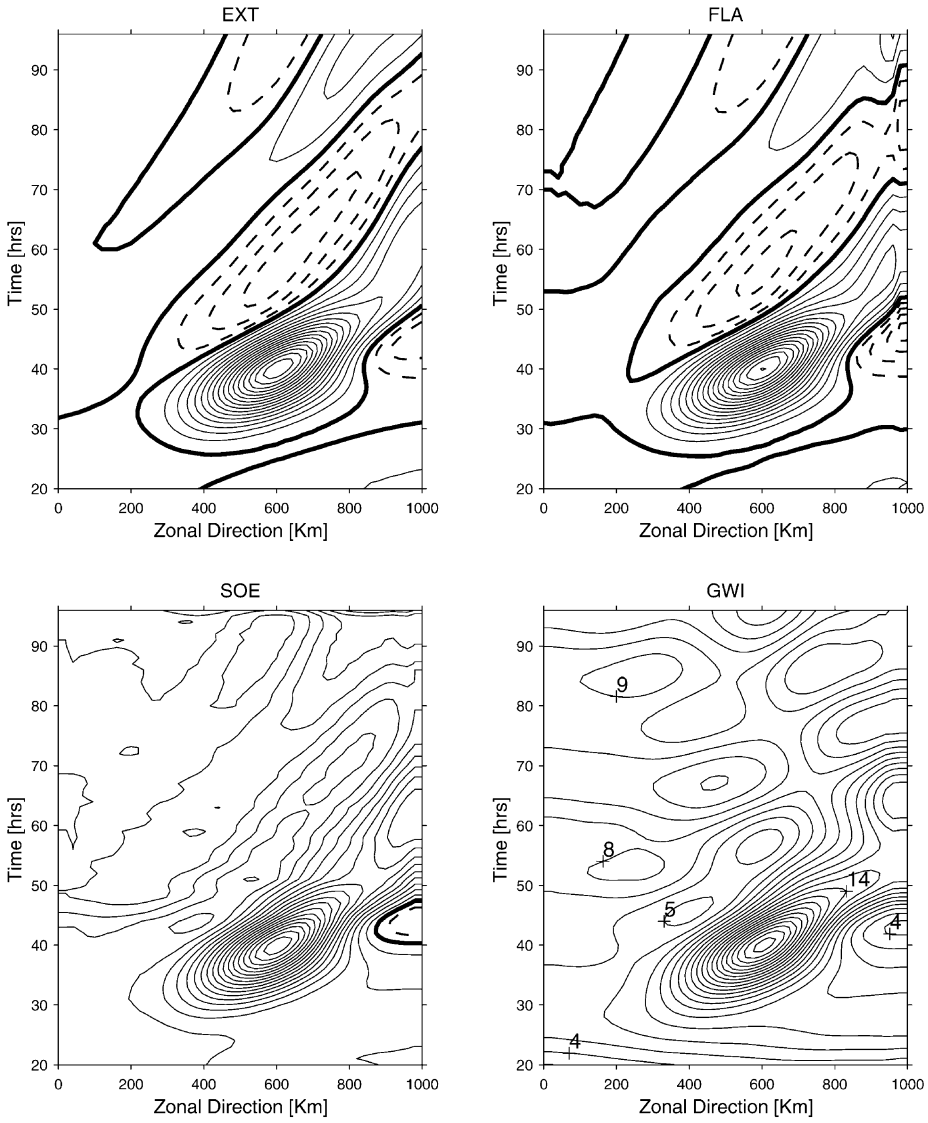

Fig. 11. Time-zonal plots of sea surface elevation along the transect $y = 20$ km for the travelling storm experiment. The upper left panel shows the result from the extended domain experiment (EXT), other panels are results obtained using the OBC scheme indicated on top of each panel. Results using ORI and SRE are similar to those of SOE. Contour interval is 1 cm, dashed lines indicate negative values and the thick solid line is the zero elevation contour. Note that the averaged mean sea level is higher than zero for the GWI scheme.

experiment). Fig. 8 shows the time evolution of the AMSL curves during the simulation time. GWI presents an oscillating behaviour with average amplitude around 5 cm, while SOE shows a maximum increase of near 60 cm. At difference with the previous experiment, in this case the use of the ICE constraint did not improve the results. Although the ICE constraint stops the artificial filling of the basin, it also creates an artificial clamping of the open boundary which reflects in spurious oscillations (Fig. 8). These oscillations eventually lead to errors that deteriorate the interior solution, as seen in Fig. 9 showing the sea surface elevation field for the corrected schemes. Travelling waves appear along

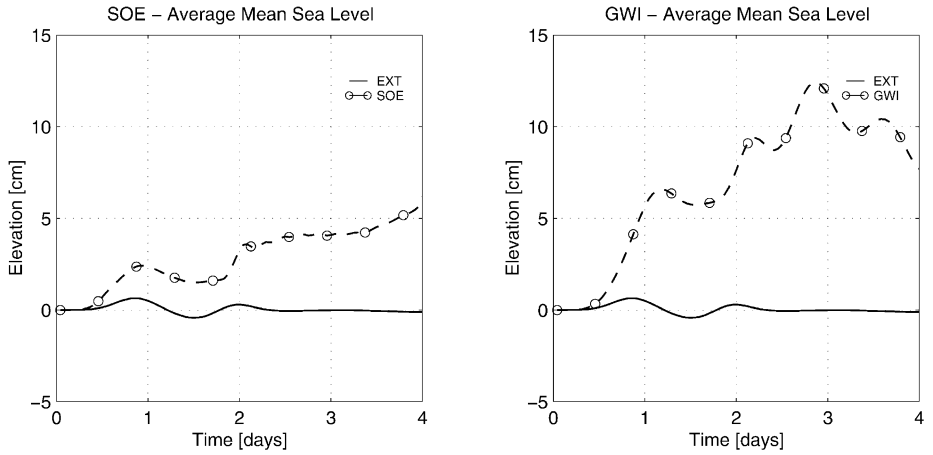

Fig. 12. Time series of area averaged mean sea level (AMSL) from the travelling storm experiment.

the eastern boundary for the SOE, SRE and ORI schemes, while the perturbation is more pronounced on the western side for GWI.

Another constraint that can be used to boost the performance of the OBCs is an integral flux constraint (ICF) of the form:

$$\int_0^W [U(H+\eta)]_{\text{west}}\,\mathrm{d}y - \int_0^W [U(H+\eta)]_{\text{east}}\,\mathrm{d}y = 0 \tag{10}$$

This constraint was employed to supplement an active boundary condition by Chang (1994) and Thompson and Schmitz (1989) among others. Fig. 10 shows the results for GWI and SOE supplemented by the ICF; now the response closely resembles the benchmark solution. Results using ORI and SRE (not shown) are similar to those of SOE. Also shown in the figure is the correct response obtained using BKI with a time scale $T_f = 1$ h (as suggested by Fig. 6).

3.3. Travelling storm experiment

In this experiment, we test the OBCs schemes in flows dominated by the simultaneous effects of direct wind forcing and wave radiation. Following Roed and Cooper (1987), we simulated the passage of a relatively strong cyclone over the channel. The wind stress has a Gaussian distribution and shape a maximum of 3 Pa. It translates at a speed of 8 m s^{-1} from the northwest to the southeast. The storm has a radius of 100 km and its centre enters the computational domain at $x = 250$ km, $y = 500$ km and $t = 20$ h. At hour 32, the storm is located in the middle of the computational domain, leaving it 12 h later at $x = 750$ km, $y = 0$.

Since there is no analytical solution to this problem, the experiments using OBCs were compared to a benchmark case conducted in the extended domain described in Section 3.2. The total simulation time was 96 h. Fig. 11 (top left panel) shows the time evolution of the free surface elevation for a slice taken along $y = 20$ km. The maximum elevation occurs at approximately hour 40, just before the storm centre hits the coast. The coastal adjustment is achieved through the propagation of surface gravity waves, high frequency edge waves propagating alongshore in both directions, and low frequency coastal shelf modes propagating in the positive x direction. The westward propagation of these waves is evident from the positive slope of the contour lines; the change in the slope between hour 40 and 50 denoting a change in phase speed. The dominance of the low-mode shelf response to cyclones can be related to the similarity in space and time scales of the forcing and these waves (Tang and Grimshaw, 1996).

The qualitative performance of the OBCs can be evaluated in Fig. 11, which shows time–longitude plots of the sea surface elevation. Of all the conditions, only FLA produces results similar to the benchmark case, albeit some tilting of the contour lines is evident near the eastern open boundary. Orlanski's type radiation conditions (only SOE is shown) show

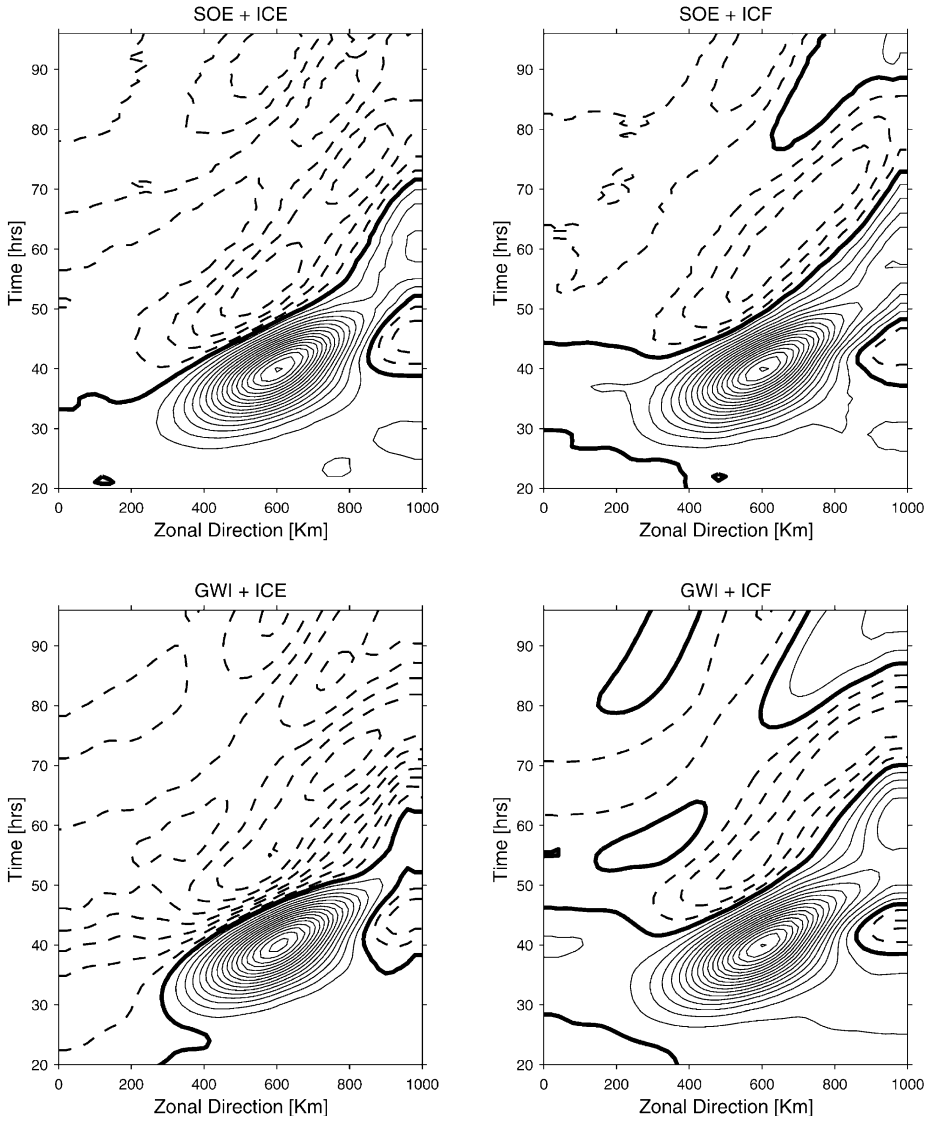

Fig. 13. As for Fig. 11 but showing results using the SOE and GWI radiation conditions boosted by integral constraints in elevation (ICE) and flux (ICF). Results using ORI and SRE are similar to those of SOE. Contour interval is 1 cm, dashed lines indicate negative values and the thick solid line is the zero elevation contour.

strong reflections, with short waves propagating inward as evidenced by the wiggling contours and slope changes after the first wave packet passes through the boundary (hour 50). GWI also exhibits reflections at the same boundary, but their deviations are more pronounced at the western boundary. The reflective behaviour of these schemes appears to be related to the highly dispersive nature of the problem, the shelf waves having large differences in phase speed. The absence of dashed (negative) contour lines in SOE, GWI as compared with the extended (EXT) solution is associated with spurious changes in mean sea level produced by the OBCs. This problem is more apparent in Fig. 12, which shows the average mean sea level (AMSL) for the GWI and SOE schemes, both displaying an artificial filling

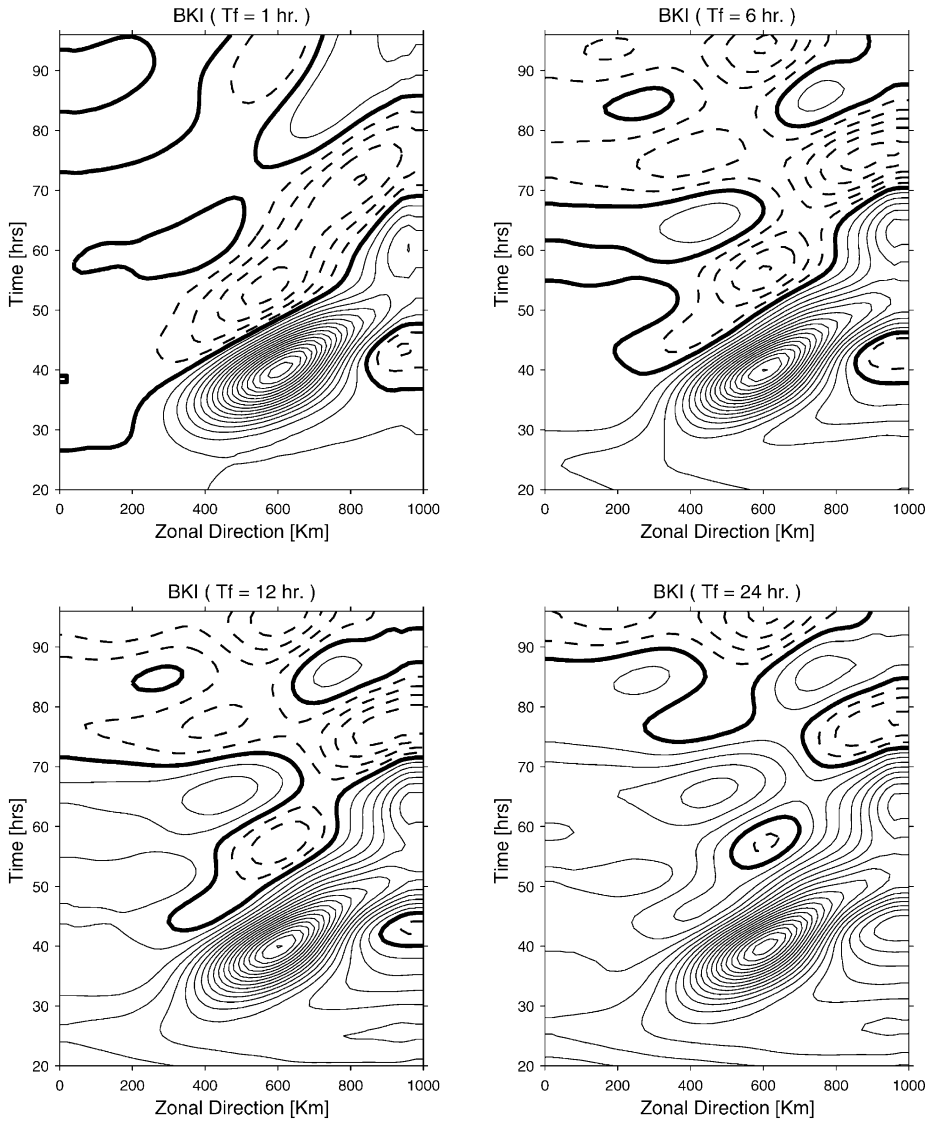

Fig. 14. As for Fig. 11 but showing results using the BKI scheme for different values of the time relaxation parameter T_f. Contour interval is 1 cm, dashed lines indicate negative values and the thick solid line is the zero elevation contour.

of the basin. FLA (not shown) conserves mass during the entire simulation.

We investigated the possibility of improving the response of GWI and SOE by imposing integral constraints on surface elevation (ICE) and transport (ICF) and by using the damped radiation condition (BKI). Fig. 13 (left panels) shows the results using ICE. In this case, the sea level is forced towards an incorrect steady state value. The ICF (right panels) improves the solution although the problems persist for both schemes, at the western and eastern boundaries of the domain. Results obtained using the damped radiation scheme (BKI) for different values of the relaxation time scale T_f are shown in Fig. 14. The best response is for $T_f = 1$ h (corresponding to the travel time of the fastest wave across the domain), although distortions of the contour lines are evident after the passage of the dispersive packets at

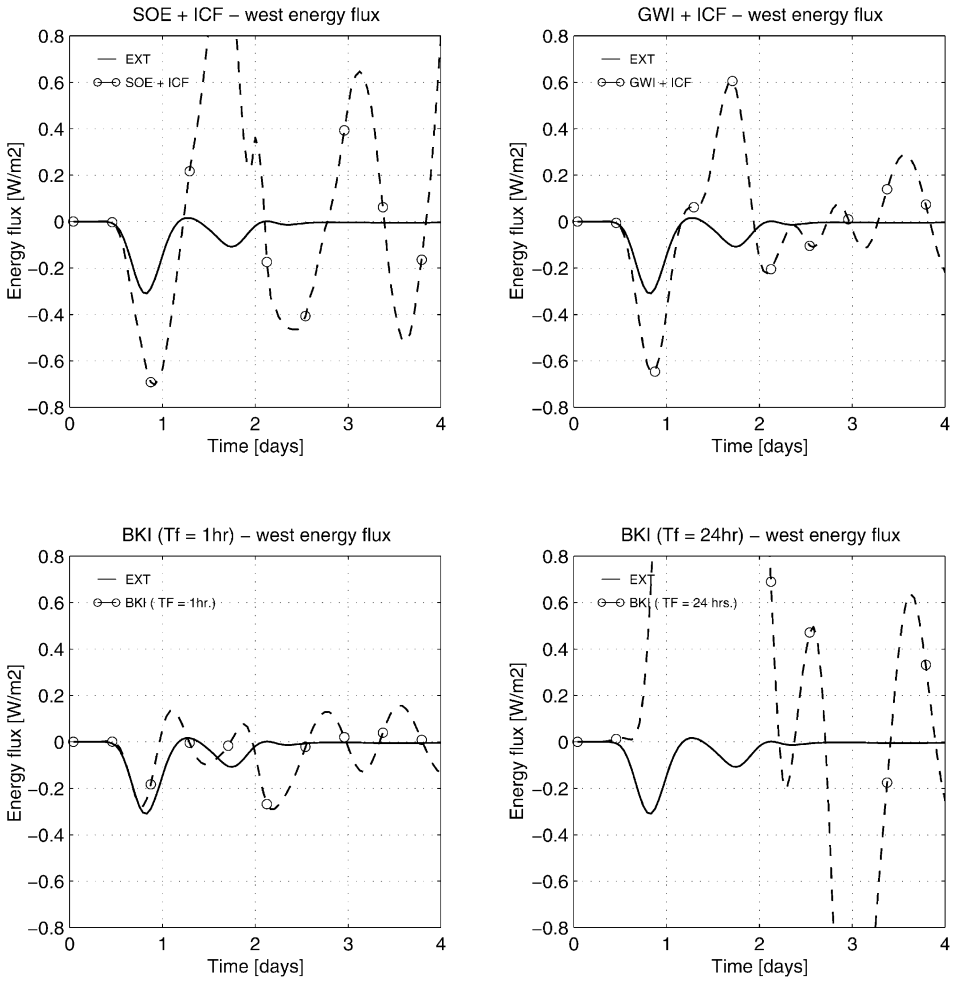

Fig. 15. Time series of west energy flux from the travelling storm experiment. Solid lines are the result from the extended domain simulation (EXT), dashed lines are results obtained using the OBC schemes indicated on top of each panel.

the eastern boundary (hour 50). Higher values of T_f further deteriorate the overall solution due to the enhanced radiation properties of the scheme (compare with the GWI panel of Fig. 11).

To further asses the OBCs' related distortions at the inflowing boundary, we calculated the energy fluxes at the western boundary. Fig. 15 shows the temporal evolution of the energy flux through the western side of the domain for the SOE and GWI schemes. Although the ICF improves the mass conservation properties of the schemes, it is clear from the figure that at the same time it perturbs the energy flux at the boundary, producing unwanted reflections. Similar conclusions can be drawn for the energy flux properties of the BKI scheme. The reflected energy accumulates inside the domain and could eventually lead to instabilities in long-term simulations if friction is not strong enough to prevent their growth.

4. Summary and conclusions

In this article, we analysed several problems associated to the implementation of different radiation OBCs in primitive equation models. The observed response included erroneous mass and energy fluxes

that ultimately deteriorated the overall interior solution. To ameliorate the problem and avoid the spurious changes in sea surface elevation and total volume, we used damped radiation conditions (BKI), integral constraints on sea surface elevation (ICE) and volume fluxes (ICF), and local solutions (LS).

In advection-dominated flows, the ICE improved the performance of SOE, ORI and GWI, while the SRE scheme did not reach a steady state even after 100 days of simulation time. A local solution approach adapted from Roed and Smedstad (1984) improved considerably the response of the FLA scheme. The BKI scheme with a relaxation time scale $T_f = 4$ days also gave a correct response, although lower values of T_f reduced the along-shore and cross-shore flows, preventing the normal evolution of the sea surface slope at the boundaries.

In cases where the oceanic response involves wave radiation of non-dispersive waves (barotropic adjustment experiment), ICE produces an incorrect oscillatory solution for the SOE scheme and a contaminated steady state for the GWI. Both results could be related to partial clamping of the open boundary induced by the ICE, and therefore, this constraint is not recommended for radiation dominated problems. In this particular dynamical setting, the use of an ICF and the BKI ($T_f = 1$ h) and FLA schemes proved to be a better alternative. Radiation conditions supplemented by an ICF have been successfully used in realistic model simulations driven by inflows/outflows at the open boundaries (Thompson and Schmitz, 1989; Chang, 1994).

For problems involving the generation of dispersive wave packets as in the travelling storm experiment, we do not recommend the use of radiation conditions with constant phase speed (GWI) or radiation conditions of the Orlanski type (SOE, ORI, SRE). The use of integral constraints for these schemes, either on free surface elevations (ICE) or volume flux (ICF), severely perturbs the flux of energy at the open boundaries and produces unwanted reflections that contaminate the interior solution. Similar results were obtained with the BKI scheme for different values of the relaxation time scale (T_f). In this type of coastal circulation models, associated with the propagation of continental shelf waves, the radiation condition type proposed by Flather (1976), although with limitations, is a better choice.

Overall FLA is the only radiation scheme that provides reasonable responses in all cases studied. It is interesting to note that the scheme has been successfully applied in simulations where the model included the effects of realistic bottom topography and wind forcing (Matano et al., 1998; Oke and Middleton, 2000) and the combined effect of wind and tidal forcing (Glorioso and Flather, 1995).

Acknowledgements

This work was supported by the Agencia Nacional de Ciencia y Tecnologia through grant PICT99 07-06420 BID 1201/OC-AR to Elbio Daniel Palma. Ricardo P. Matano acknowledges support by NSF Grants OPP 9527695 and OCE-9819223. The technical and financial support of Universidad Nacional de Sur (Argentina) is also gratefully acknowledged.

References

Blumberg, A.F., Khanta, L.H., 1985. Open boundary conditions for circulation models. J. Hydraul. Engng. 11, 237–255.

Blumberg, A.F., Mellor, G.L., 1987. A description of a three-dimensional coastal ocean circulation model. In: Heaps, N. (Ed.). Three-Dimensional Coastal Ocean Models. Coastal Estuarine Science 4. AGU, Washington, DC, pp. 1–16.

Chang, K.Y., 1994. Open boundary conditions for a channel model. Ocean Res. 16, 75–93.

Chapman, D.C., 1985. Numerical treatment of cross-shelf open boundaries in a barotropic coastal ocean model. J. Phys. Oceanogr. 15, 1060–1075.

Flather, R.A., 1976. A tidal model of the northwest European continental shelf. Mem. Soc. R. Sci. Liege, Ser. 6 (10), 141–164.

Glorioso, P.D., Flather, R.A., 1995. A barotropic model of the currents off SE South America. J. Geophys. Res. 100 (C7), 13427–13440.

Hayashi, T., Greenberg, D.A., Garrett, C.J.R., 1986. Open boundary conditions for numerical models of shelf sea circulation. Cont. Shelf Res. 5, 487–497.

Johnsen, M., Lynch, R.D., 1995. Assessment of a second-order radiation boundary condition for tidal and wind driven flows. In: Lynch, D.R., Davies, A.M. (Eds.). Quantitative Skill Assessment for Coastal Ocean Models. Coastal Estuarine Studies 47. AGU, Washington, DC, pp. 49–70.

Matano, R.P., Palma, E.D., Mesias, J.M., Strub, P.T., 1998. Open boundary conditions for use in coastal models. In: Spaulding, M., Blumberg, A. (Eds.). Estuarine and Coastal Modelling. ASCE, Virginia, pp. 541–555.

Miller, M.J., Thorpe, A.J., 1981. Radiation conditions for the lateral

boundaries of limited-area numerical models. Quart. J. R. Met. Soc. 107, 615–628.

Oke, P.R., Middleton, J.H., 2000. Topographically induced upwelling off Eastern Australia. J. Phys. Oceanogr. 30, 512–531.

Orlanski, I., 1976. A simple boundary condition for unbounded hyperbolic flows. J. Comput. Phys. 21, 251–269.

Palma, E.D., Matano, R.P., 1998. On the implementation of passive open boundary conditions for a general circulation model: the barotropic mode. J. Geophys. Res. 103 (C1), 1319–1341.

Roed, L.P., Cooper, C., 1987. A study of various open boundary conditions for wind-forced barotropic numerical ocean models. In: Nihoul, J.C.J., Jamart, B.N. (Eds.). Three-Dimensional Models of Marine and Estuarine Dynamics. Elsevier, Amsterdam, pp. 305–335.

Roed, L.P., Smedstad, O.M., 1984. Open boundary conditions for forced waves in a rotating fluid. SIAM J. Sci. Stat. Comput. 5, 414–426.

Sommerfeld, A., 1949. Partial differential equations. Lectures in Theoretical Physics 6. Academic Press, New York.

Tang, Y., Grimshaw, R., 1996. Radiation boundary conditions in barotropic coastal ocean numerical models. J. Comput. Phys. 123, 96–110.

Thompson, J.D., Schmitz Jr., W.J., 1989. A limited-area model of the Gulf-Stream: design, initial experiments, and model-data intercomparison. J. Phys. Oceanogr. 19, 791–814.

Vastano, A.C., Reid, R.O., 1967. Tsunami response for islands: verification of a numerical procedure. J. Mar. Res. 25, 129–139.